Shear failure characterization in masonry components made with different mortars based on combined NDT methods

G. Livitsanos [a],*, N. Shetty [b], E. Verstrynge [b], M. Wevers [c], D. Van Hemelrijck [a], D.G. Aggelis [a]

[a] Dept. Mechanics of Materials and Constructions, Vrije Universiteit Brussel, Brussels, Belgium
[b] Civil Engineering Department, Building Materials and Building Technology Division, KU Leuven, Leuven, Belgium
[c] Dept. of Materials Engineering, KU Leuven, Leuven, Belgium

HIGHLIGHTS

- AE fracture mode characterization of masonry constituents.
- Successful correlation between full-field strain pattern from DIC with AE indices in masonry components.
- Shear fracture mode characterization.
- FEM numerical simulation.

ARTICLE INFO

ABSTRACT

In this paper, an experimental study conducted on Red Clay brick masonry "triplets" built with Cement and Lime-based mortars is presented. Monitoring of fracture is executed by Acoustic Emission (AE) and Digital Image Correlation (DIC). First, for a profound understanding of individual properties, small scale experiments were conducted for characterization of AE signatures of mortar and brick separately. Representative masonry triplet elements are tested in shear for investigation of the fracture mechanisms in relation to the properties of different mortars. Localization of the cracks as well as source identification is performed by means of AE parameter-based analysis. Their correlation with DIC, accurately showed the location of macro cracking and the developing of strain concentrations even before fracture. This is one of the first investigations where full field strain pattern from DIC are successfully correlated with AE indices in masonry. Numerical simulations were also performed for validation and prediction purposes.

1. Introduction

A large number of historical structures are built up in masonry. Brick masonry is a heterogeneous and anisotropic material formed by bricks and mortar. Its behavior up to failure is nonlinear and primarily depends on its components (brick, mortar and brick-mortar interface). Characterization of its material properties and structural condition is necessary for repair and conservation aiming to a long and safe service life [1–3]. Mortars play a significant role in the masonry's overall performance. The primary purpose of mortar in masonry is to bond masonry units into an assemblage which acts as an integral element having desired functional performance characteristics [4]. Because Portland cement concretes and masonry mortars contain some of the same principal ingredients, it is often erroneously assumed that good concrete practice is also good mortar practice. Realistically, mortars differ from concrete in working consistencies, in methods of placement and in the curing environment. According to masonry mortar standards [5], mortars should typically be weaker than the masonry units, so that any cracks will occur in the mortar joints where they can more easily be repaired. In addition, the bed joint thickness exercises certain influence on the masonry's overall performance. The compressive strength of mortar depends largely upon the binder content, binder type, the binder-cement and the water-cement ratio. It increases with an increase in binder ratio, with cement-based mortars usually considered to have higher strength than lime-based mortars. However, compressive strength should not be the sole criterion for mortar selection. Bond strength is generally the most important factor but also flexural strength because it measures the ability of a mortar to resist cracking. The tensile and compressive strength of mortar usually exceeds the bond strength between the mortar and the masonry unit. Mortar joints, therefore, are subjected to bond failures at lower tensile or shear stress levels. A lack of bond

---

* Corresponding author.
   E-mail address: Georgios.livitsanos@vub.be (G. Livitsanos).

at the interface of mortar and masonry unit, e.g. due to shrinkage, may lead to moisture penetration through those areas. Consequently, many different ways have been proposed for strengthening unreinforced masonry structures [6]. However, it is always important to investigate and get a profound knowledge of the brick-mortar interaction under all different kind of excitations in order to assess and propose the most suitable strengthening concept according to each specific case.

In this study, the effect of different mortar compositions on the masonry's structural behavior is examined. The correct identification of several mechanical parameters is required to characterize masonry material. The shear strength of masonry triplets, (for instance under zero normal stress), is one of these parameters [4,7,8]. In masonry, shear forces are undertaken dominantly by the mortar joints. As a result, the interface cohesion and the exact definition of the mortar properties, play a crucial role in the prediction of masonry behavior under any kind of action. In this research, cement- as well as lime-based mortars are investigated. On one hand, the cement mortar contributes strength and durability to masonry but on the other hand, it lacks plasticity rendering it vulnerable to cracking.

However, lime mortar, either combined with cement mortar into a hybrid mortar or used as a pure lime mortar, provides certain plasticity to the whole masonry and a better adhesion with the bricks. Evaluation of the behavior is conducted by use of NDT techniques. The use of Acoustic Emission (AE) technique and Digital Image Correlation (DIC) is addressed. AE is a powerful technique for detection and analysis of the elastic waves produced by the failure mechanisms [9–13]. The localization of the cracks as well as the source identification of the micro cracks and by means of AE analysis give a clear view on the crack initiation and propagation in small and large scale [14–16]. DIC technique provides the surface full-field strain maps, and the necessary validation for AE results in such a heterogeneous system as masonry [17–20]. As shown in a previous study [21], even in the case of axial compression, local cracking may be produced by a variety of stress components that include strong shear, confirmed by transient DIC strain maps and AE parameters. In this paper, shear loading in triplets is addressed, forming a stress pattern which depends on the mechanical properties of the binding material. Results with a focus on a characterization of the AE fracture modes on mortar beams as well as masonry triplets, both subjected to shear dominated failure, are presented. For both specimen types, four different mortar compositions are considered.

2. Experimental details

2.1. Materials

This paper focuses on the mortar contribution. Therefore, four mortars and one type of brick were chosen, the properties of which depend on the different compositions (Fig. 1[a], [b]). Specifically, Cement based mortar (CM), Lime-Cement (LC), Lime Hydrate (LH) and Hydraulic Lime (HL) mortars were chosen (Table 1). The binder over aggregate (B:A) values are derived from practical experience and are comparable to values given in various national standards. For the prefabricated blended binder HL, it is in agreement with the producer's guidelines. Water over Binder (W:B) values have been determined for optimum workability. The preparation of the sand, the adding order of the components and the mixing is important. The sand is dried in 80 °C for three days for all compositions. In the case of (HL) the grade of NHL5 is used. The NHL - stands for Natural Hydraulic Lime. The number relates to compressive strength in N/mm². In case of (LC), Supercalco90 (CL90S) is mixed with cement and it acts as a plasticizer. Hydrated lime contributes to workability, water retention, and elasticity. It is a building lime according to EN 459-1, recommended for all types of masonry, with good adhesion and excellent early strength. Finally, in the case of Lime Hydrate (LH) mortar, only lime CL90S is used. Binder HL hardens due to hydraulic reaction and LH primarily due to carbonation. Lime mortars carbonate gradually under the influence of carbon dioxide in the air. Because of this, complete hardening occurs very slowly over a long period of time. This allows healing, the re-cementing of small hairline cracks. The influences of carbonation implications are also studied by Verstrynge [22] and Ferretti [23].

The mortar specimens were cast according to the standards [25] with dimensions 40 × 40 × 160 mm. Six specimens in total of each mortar type were representative for investigating each material's mechanical and AE properties. Three of each type, were subjected to three point-bending tests. A slight modification was done for the remaining three mortar specimens of each mortar mixture in order to investigate the "shear" fracture mode (Fig. 2[b]) [21].

Fig. 1. Visual aspect of [a] Red Clay Brick (RCB) and [b] Mortar specimens (CM – LC – LH – HL).(For interpretation of the references to colour in this figure legend, the reader is referred to the web version of this article.)

Table 1
Composition of Mortars, according to [24].

Composition	Lime Hydrate (LH)	Hydraulic Lime (HL)	Lime –Cement (LC)	Cement (CM)
River Sand (g)	2700	2700	2700	2700
Binder (g)	342.9	572.4	572.5	666.9 CEM I 42.5 R, Portland cement
	CL90S	NHL5	66.7% CL90S (EN 459-1:2001)	
	(EN 459-1:2001)	(EN 459-1:2001)	33.3% CEM I 42.5 R	
Water at 20 °C (g)	620.6	630.8	583.3	604.9
Volume density (kg/m³)	1662	1746	1758	1960
B:A (kg/kg)	0.120	0.212	0.212	0.247
W:B (kg/kg)	1.809	1.102	1.018	0.907
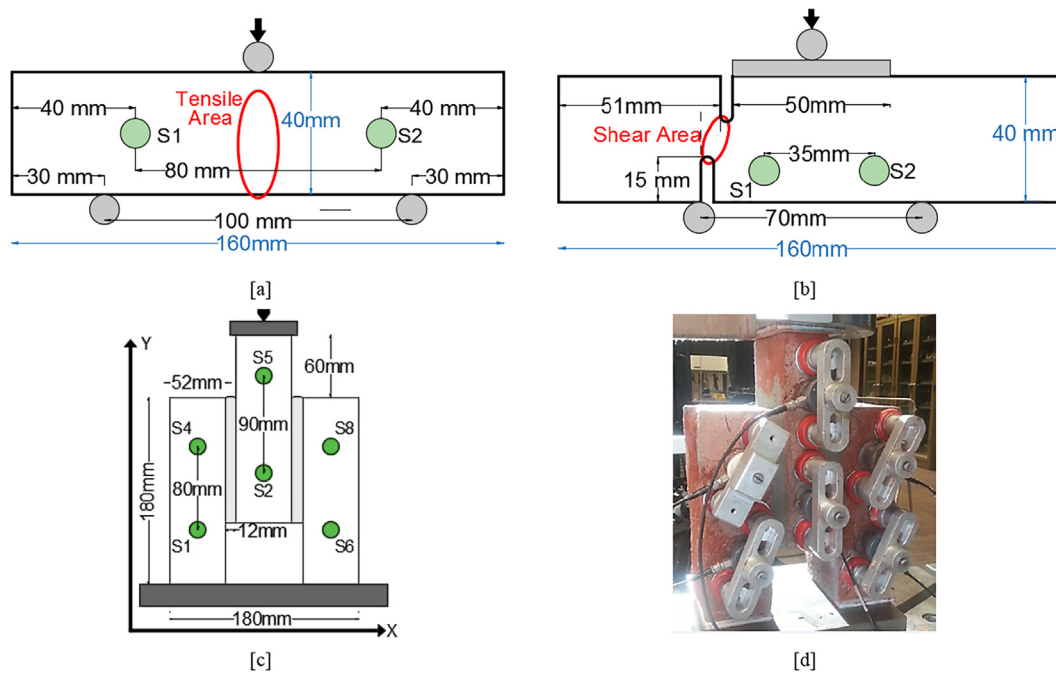
Fig. 2. [a] Test setup for mortar beams under three-point bending (side view), [b] mortar beams under shear dominated failure, [c] masonry triplets for shear testing. Green dots indicate AE sensors' position, [d] AE applied on specimen's surface for measurements.(For interpretation of the references to colour in this figure legend, the reader is referred to the web version of this article.)

The brick is a typical solid Red Clay Brick (RCB) with a density 1653 kg/m^3 and dimensions $188 \times 88 \times 63$ mm^3, which is representative for historical masonry because of the mechanical properties, the color and the surface roughness. The aforementioned procedure for the mortars was also followed in the RCB where three brick beam specimens were cut to the size 40x40x160 mm for flexural tests and three others for "shear" failure. Furthermore, three triplet masonry elements for each type of mortar were prepared where three bricks were assembled with two mortar joints in a configuration as is shown in Fig. 2[c], [d]. These specimens are used with the aim to characterize the shear behavior, while the compressive behavior of "couplets" was recently examined [21]. Before applying the mortar layers, the bricks were submerged in water for two minutes to avoid absorption of the mortar's water into the pores of the bricks. During testing, the load was applied using an Instron 5885 testing machine with a 250 KN capacity load cell. For the flexural and the shear dominated tests on mortars the loading rate was at 0.2 mm/min in agreement with shear tests on triplets where the rate was also 0.2 mm/min. In all cases, the loading was displacement controlled.

2.2. Measurements

All the brick and mortar beam specimens described in Section 2.1, were subjected to direct Ultrasonic Pulse Velocity measurements (UPV) before the bending and shear dominated tests. A portable Ultrasonic Pulse Analyzer apparatus by Controls Group, with 2 MHz sampling rate, 2500 V and 50 kHz transmitter pulse was applied. In each specimen, 2 velocity measurements were conducted in the longitudinal and 2 in the transversal direction for testing the measurements' consistency and a possible heterogeneity. Furthermore, UPV measurements were also conducted along the width of the triplet specimens in order to obtain the initial elastic wave velocity before fracture. This was used as a reference input also during the AE acquisition for event localization.

For the second series of experiments, mortar beams were subjected to flexural and shear dominated failure tests with the concurrent monitoring of the total AE activity and linearly locating the AE events (Fig. 2[a], [b]). For the AE monitoring, piezoelectric sensors (R15α, with 40 dB preamplifier) with resonant frequency 150 kHz were used. The threshold was 35 dB. Finally, in the case of triplets, AE planar location was applied by six sensors where 2 sensors were placed on each of the three bricks on either sides of the mortar joints (Fig. 2[c]). Acoustic coupling was improved by Vaseline (petroleum jelly) between the sensors face and the specimens' surface. Some of the main recorded AE signal features are the maximum Amplitude, A (usually in dB), and the duration (period between the first and the last threshold crossing). The Rise Time, RT (which is the time between the first threshold crossing and the point of peak Amplitude in μs) is related to the fracture mode of the crack [9]. Frequency content can be simplified to AF (Average Frequency), which is the total number of threshold crossings divided by the duration [9].

Moreover, a Digital Image Correlation (DIC) system with two high-resolution cameras was applied on the other side of the triplet specimens. A random black-white speckle pattern was applied using aerosol paint, (see Fig. 2[d]) to obtain the full-field strain maps during testing through triangulation of the two cameras. Capturing images constantly of the deformed (due to loading) sprayed pattern on the specimens' surface, the specimens' in-plane deformations were calculated. Their gradients, strains ε_{xx} (perpendicular to loading direction) and ε_{yy} (parallel to loading) are correspondingly determined. Apart from the normal strains, the shear strain ε_{xy}, which represents the changes in the angle with respect to the x and y direction, is calculated [26].

Finally, it is worthy to mention that the displacement accuracy depends on the resolution of the DIC cameras, on the distance of the specimen from the cameras and on the "subset" size. The subset size controls the area of the image that is used to track the displacement between images and it must be large enough to ensure that there is a sufficiently distinctive pattern contained in the area

used for correlation. Due to the large size of the specimen's monitored area and the distance between the cameras and the specimen, a subset size of 21 pixels with a step size of 7 was selected for accurate strain calculations. In the experiments discussed in this paper the best possible displacement accuracy was calculated to be approximately ±4.2 μm.

3. FEM analysis

Static FEM simulations of the triplet specimens were conducted for acquiring a robust comparison of the strain ratio outputs from DIC with the ones from the numerical simulations of the selected setup. The resulting stress condition for the "shear" test is shown in Fig. 3. Firstly, for the FEM analysis, a convergence analysis was conducted in order to guarantee a numerically stable simulation. The parameter that was investigated for the convergence analysis was the vertical displacement along the load direction.Fig.

For the stress calculation, solid deformable elements in three dimensions of the C3D8R type were used. This is a standard element of Abaqus with eight contact nodes. The "approximate global size" was finally set to 1.5 mm for the mortar joints areas where the main area of interest is, and 3 mm for the brick elements. The "approximate global size", used by the software to control the density of mesh seeds throughout the specimen, is inversely proportional to the number of elements included in the mesh structure. Finally, each mortar joint was simulated with 38,400 and each brick with 32,400 elements, resulting in a resolution of 1.5 mm for mortar and 3 mm for brick. Elastic modulus of 2.5 GPa was selected for the brick component while different
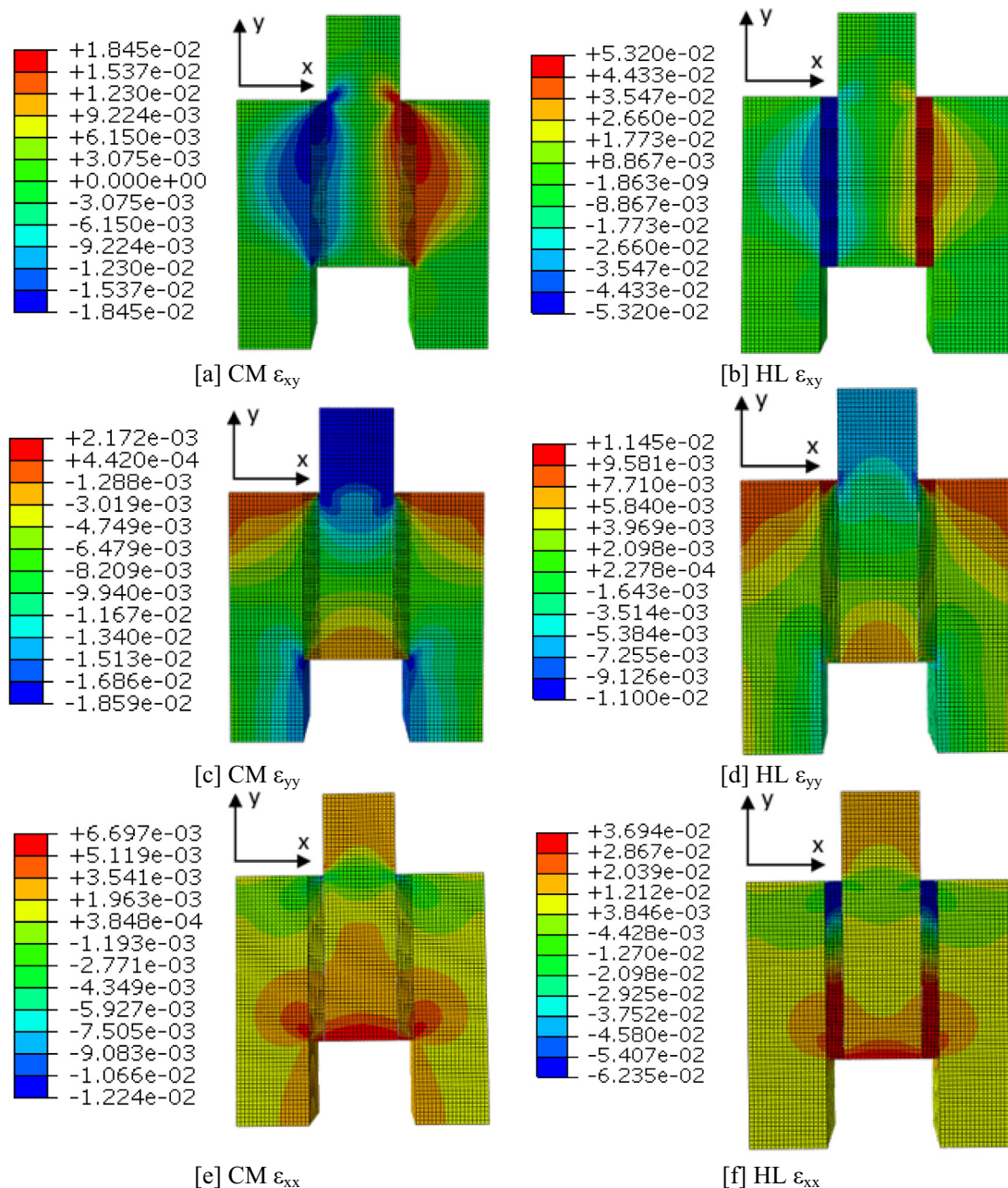
Fig. 3. [a] Shear ε_{xy}, [c] Vertical ε_{yy}, [e] Horizontal ε_{xx} strain distribution of CM triplet, [b] Shear ε_{xy}, [d] Vertical ε_{yy}, [f] Horizontal ε_{xx} strain distribution of HL triplet calculated with FEM software for the shear dominated failure.

Table 2
Mean values of UP velocities m/s.

	Specimen	Wave Velocity [m/sec]	Young's modulus [MPa]
Red Clay Brick	RCB	1250–1351	2508
Mortars	Cement (CM)	2527–3514	4735
	Lime Cement (LC)	923–1036	1050
	Lime Hydrate (LH)	907–1015	645
	Hydraulic Lime (HL)	634–752	410
Triplets with binder of:	Cement – RCB	1267–1448	
	Lime Cement – RCB	997–1234	
	Hydraulic Lime – RCB	954–1137	
	Lime Hydrate – RCB	856–1084	

values were assumed for the mortar joints. For this approach, Poisson's ratio was taken as 0.2 for all elements. These values were obtained from compression tests on brick and mortar cubes and parallel DIC surface strain monitoring (Table 2). The applied displacement in the FEM model at the top of the middle brick, was indicatively 2 mm vertically in the middle brick in the y axis for all of the different cases following the average value of the final displacements in the lab-scale experiments. The selection of the displacement is indicative and is used to check the distribution of strains for different types of binder. The exact value of strain would change linearly with different imposed displacement. The experimental maximum values of the load displacement curves of the following Fig. 6 [b], [c] with their characteristic failure patterns are presented in Table 3.

Moreover, it is highlighted that this is an elastic simulation that does not take into account possible cracking. Furthermore, as the main interest is in the simplified linear constitutive behavior of the specimens before unstable stress strain redistributions occur, the connection between the different materials is assumed "rough" signifying as zero the relative movement in the connected surfaces. Therefore, a "rough" connection is made between the materials. According to the ABAQUS manual, when a rough connection is assumed, there is no bound on the shear stress or in other words no relative motion can occur if the surfaces are in contact [27]. In the models, the connection between the bricks' and mortar layers' surfaces are defined with the "surface-surface" Abaqus option, specifying "master" and "slave" surfaces. The difference relies on the strength and stiffness of the materials meaning that the material with the highest strength and stiffness cannot be penetrated by the lower properties unit, and as a consequence it is defined as "master" surface. The interaction between the surfaces was defined for longitudinal and transversal behavior. All the aforementioned steps apply for all the different cases described in this paper.

In Fig. 3, difference in the evolution of all the strain components ε_{xx}, ε_{yy}, ε_{xy} is observed between different triplet compositions. This relies on the difference of the elastic modulus of bricks and mortar joints which affect the strain evolution and distribution. For instance, in case where the joint is stiffer than the brick [a], [c], [e], stresses are distributed to wider area compare to the less stiff mortars where the large deformability of the joints results in strain concentrations dominantly in these areas (Fig. 3[b], [d], [f]). This first strain field observation, is encouraging for continuing in more profound strain analysis and validation with experimental full field strain map by DIC in Section 3.3.

4. Results

4.1. Ultrasonic pulse velocity testing

Ultrasonic pulse velocity was correlated with the flexural strength of each mortar type and the brick (Fig. 4). The mean wave velocity calculated by the UPV and the elastic modulus as calcu-
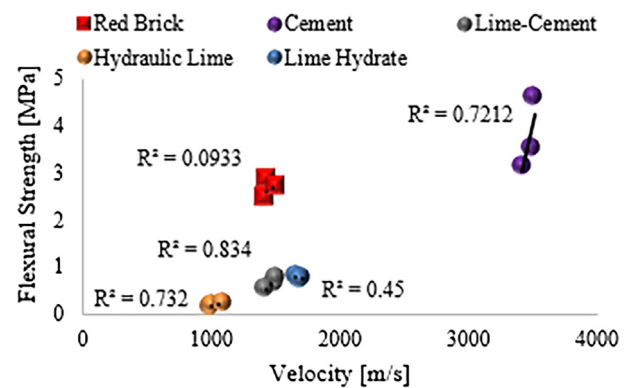
Fig. 4. . Flexural strength-velocity for Mortars and RCB.

lated by DIC under compression tests are presented in Table 2. Moreover, UPV measurements were performed on the triplet specimens in order to use the initial estimated velocity value as an input in the AE software for better location accuracy. The results for each mortar type and for the brick seem to have a consistency without large fluctuations. Furthermore, the velocity measurements in the masonry triplets, for most of the mortar compositions, seem to present values among the values of the individual constituents respectively, because of the two mortar interfaces which are inserted for assembling the bricks and the larger size of the brickwork which scatters the signal.

4.2. AE results from flexural and shear dominated bending tests

Flexural and shear dominated bending tests were performed on mortar specimens with the test set-up as shown in Fig. 2[a], [b]. In Fig. 5[a], the flexural-shear loads and the cumulative AE events as a function of time are presented for one representative specimen. The aim of this graph is not to accurately present each AE and load curve but to describe the way that different AE event clusters were selected before the final failure. The clusters, were selected as follow: Cluster I was obtained at 0–20% of the maximum load, Cluster II at approximately 40–60% while cluster III at 80–100% of the maximum load. The AE data recorded pre-peak, in the time interval close to fracture (stage 3 – see Fig. 5[a]), are extracted and analyzed in terms of important features of AE which highlight different aspects of the fracture process, such as the damage mode. In all of the tests, approximately 1100–1800 AE events were extracted for analysis and comparison. In total, three specimens were tested for each different material and each different type of failure. Consequently, in Fig. 5[b], each symbol (rhombus or triangle) corresponds to the average signal properties of all events extracted in stage 3 for each specimen. In literature, the inverse simultaneous shift between lower and higher values of rise time (RT) and average frequency (AF) has been proven efficient for characterization of the
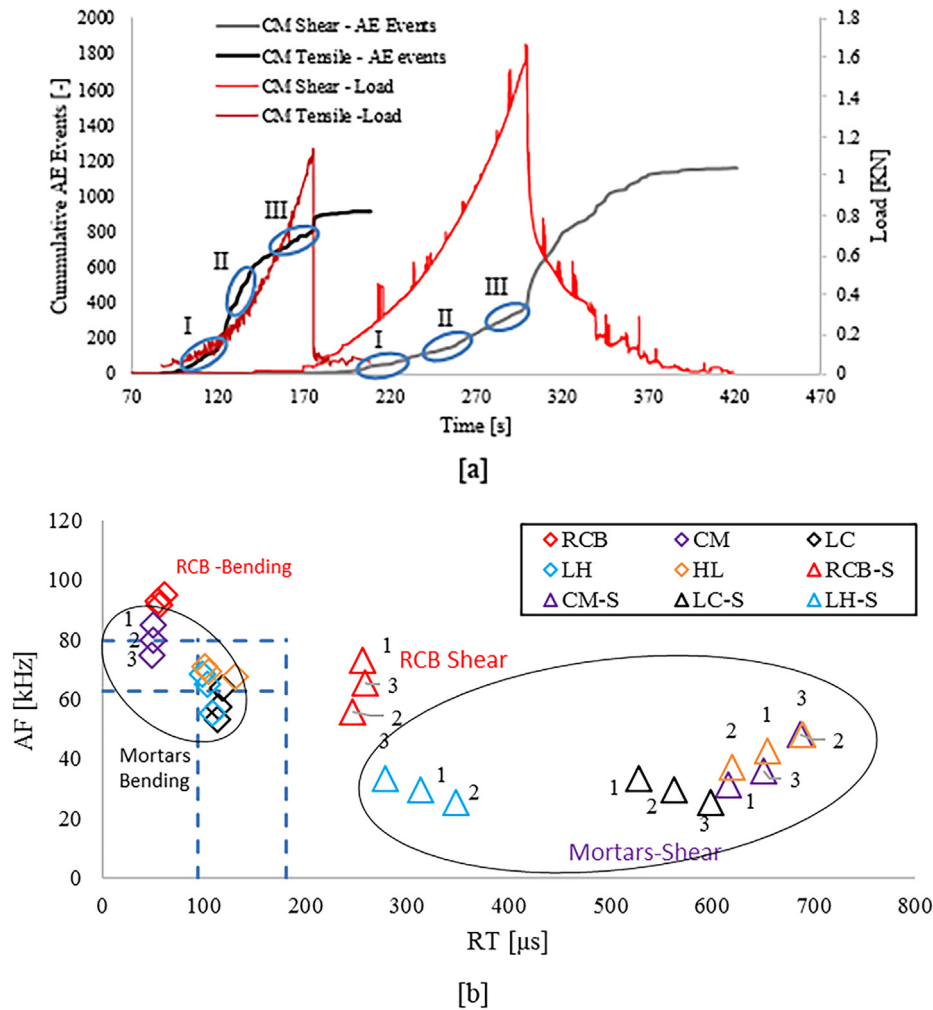
Fig. 5. [a] Indicative Acoustic Emission parameters analysis for mortar and brick beam specimens under flexural and shear dominated tests. [b] AF – RT correlation graph – Blue dashed rectangle area (94.48–180.36 RT, 62.56–79.51 AF) denotes the AE characteristics of the triplet specimens.(For interpretation of the references to colour in this figure legend, the reader is referred to the web version of this article.)

cracking mode [28–31]. Thus, after the classification, mortars and brick are compared in terms of AE parameters such as RT and AF (Fig. 5[b]). In the graph (Fig. 5[b]), the specimens imposed to a flexural failure mode are denoted by rhombus symbols while the specimens that failed under shear mode are depicted with triangular symbols. In similar fashion to the classification proposed by the Rilem recommendation [31] it is seen that the bending AE activity of bricks presents higher AF and lower RT than LC, LH and HL mortars. This is encouraging as it shows that fracture of the individual constituents (RCB – LC, LH, HL mortars) has distinctly different characteristics. This may enable fracture characterization in masonry composed by these constituents. However, in the case of CM mortar, this differentiation with RCB is smaller for specimens subjected to flexural failure.

Concerning the separation between different modes, it is also obvious that bending and "shear" (or mixed mode) tests for the same material can be distinguished. For bricks, bending is manifested by an average AF of 90.4 kHz and rise time of 36.8 µs, while mortars have an average AF of 69.6 kHz and RT of 99.5 µs respectively. For shear dominated tests, AE indices in the brick and mortar beams result in much different AE parameters. AE signals from RCB specimens under shear present an AF of 65.3 kHz and RT of 203 µs. In the case of mortar specimens, AF and RT vary between 28.5–48.3 kHz and 198–689 µs respectively. As a result, there is a decrease in AF of 44.8% and an increase of 345% in RT when comparing tensile with shear fracture in mortar specimens. Consequently, based only on these two parameters of AF and RT, it is possible to discriminate between the two modes of fracture in mortar beams or in bricks. Although this is encouraging for fracture characterization purposes, it should not be taken for granted that the separation holds for more complex systems (like triplets), rendering the aid of DIC necessary.

4.3. AE results and planar location on triplets in correlation with DIC

In Fig. 6[a], [b], the shear stress time histories of the masonry triplets are depicted. The specimens with cement mortar present the highest mean shear strength of 1.12 MPa, and the highest shear stiffness. On the other hand, LC, HL and LH masonry specimens present similar shear strength of 0.17 MPa, 0.11 MPa and 0.044 MPa respectively. These quite low values imply that the strength of the mortar material is not always reached when testing the triplet. This was confirmed by loading tests on mortar specimens focused on shear, which resulted in higher ultimate values. The shear strength was not exceeded on the triplet due to the contribution of other damage modes like debonding in the interface of the mortar joint with the brick as well as in some cases fracture of the brick, which was confirmed by DIC as it will be seen later in the same section.
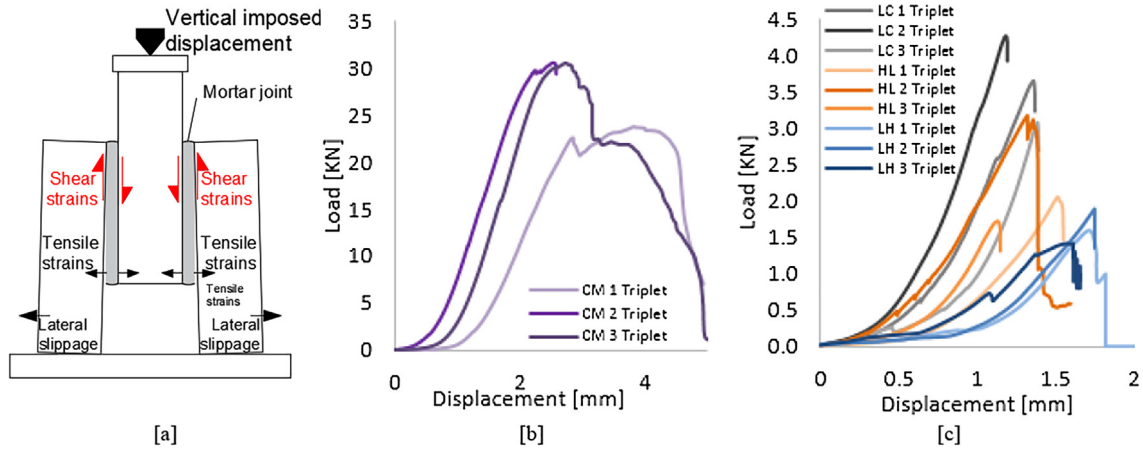
Fig. 6. [a] Gradual failure time history [b] Load – displacement curves of CM triplets, [c] Load -Displacement curves of LC, HL, LH Triplets.

Table 3
Maximum load and displacement values of the triplet specimens with the respective type of fracture.

	LOAD	DISPLACEMENT	Main type of fracture
CM1	23.76	2.56	Interface adhesion failure
CM2	30.56	2.77	Adhesion failure with crack penetration in the brick
CM3	30.53	2.85	Adhesion failure with crack penetration in the brick
Average	28.28	2.73	
STDEV	3.92	0.15	
LC1	3.65	1.19	Interface adhesion failure with short diagonal crack propagation through the mortar
LC2	4.27	1.35	-Similar-
LC3	3.07	1.37	-Similar-
Average	3.66	1.30	
STDEV	0.60	0.10	
HL1	2.05	1.32	Long diagonal cracks through the mortar
HL2	3.17	1.16	-Similar-
HL3	1.72	1.45	-Similar-
Average	2.31	1.31	
STDEV	0.76	0.15	
LH1	1.56	1.26	Interface adhesion failure with short diagonal crack propagation through the mortar
LH2	1.89	1.40	-Similar-
LH3	1.42	1.46	-Similar-
Average	1.62	1.37	
STDEV	0.24	0.10	

Masonry triplets were tested without lateral confinement and the shear stress time history was determined in accordance with the European Testing Standard EN 1052-3 [32]. The strains measured with DIC around the crack initiation area on the triplets presented a clear overview of the evolution of cracking and the magnitude of the strains (Fig. 7[a]). The window selection was done by trying to include the whole strain evolution due to the crack propagation and usually from the bottom where the crack/ strains initiated up to an upper level where the strains still were not affected by the averaging. The width of the selection window was 8–10 mm, so it included 4–5 mm of each side of the crack. In specific cases that the crack did not propagate in a straight line,
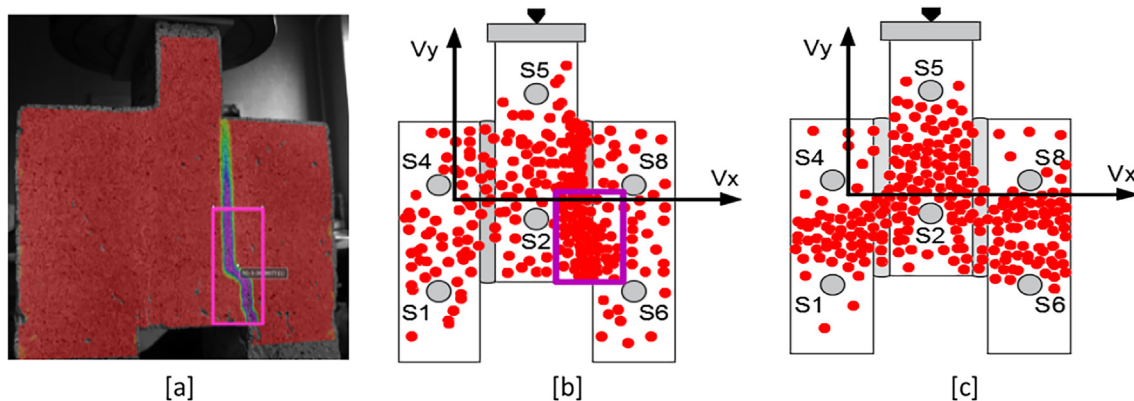
Fig. 7. Crack evolution on triplet, based on [a] DIC strain ε_{xx} profiles and [b] AE events planar orthotropic localization on the X-Y plane – extraction of strains and localized events from indicated cracked area, [c] AE events planar isotropic localization.

smaller continuous windows were assumed in order to avoid again averaging of strains. Localized AE events were extracted from the same area of interest and analyzed on the basis of AE signal parameters (Fig. 7[b]). Due to the specific geometry of the triplet, the vertical wave velocity equals the brick velocity while the horizontal one is affected by the interference of the two mortar joints and the interface properties. As a result, it was important to assume that the masonry is an orthotropic medium, for more accurate calculation of the AE events location. Consequently, different vertical and horizontal velocities were used for the planar anisotropic localization. An example concerning one of the triplet compositions (CM) is presented in Fig. 7. The formation of the cracks during fracture highly reduces the horizontal velocity. Thus, lower values than the undamaged specimen were assumed as seen in Table 4, in comparison with Table 2.

In Fig. 8, representative results are presented out of the six tested specimens for each mortar type. As a first approach, we

could observe that there are increasing strain values as the mortar composition is being altered from pure cement to lime based. In detail, in Fig. 8, this behavior is observed concerning the different strain components (ε_{xx}, ε_{yy}, ε_{xy}), with the case of hydraulic lime mortar joint (Fig. 8[d]) presenting a steady accentuated difference in the ε_{yy} component compare to ε_{xy}. Similar behavior is observed also in the graphs which describe the AE events characteristics arisen from the same area of interest. Firstly, discrete decrement of RT and increment of AF values are observed in time intervals close to fracture. Also, it is shown that RT and AF time histories present a steady decreasing and increasing trend respectively in each individual experiment despite the steady increase of the shear strain. Due to this contradiction, it was important to investigate the strain ratios, arisen from two different stages during the DIC monitoring. The first time interval is approximately around 70–80% of the maximum load, where significant strains have been developed without being significantly affected by the formation of cracks and a second interval prior to final failure around 95–100% of the maximum load. Moreover, for comparative reasons, a numerical simulation was deemed appropriate for comparison of the strain distribution. These simulations, as shown in Section 2.3, are representative of the triaxial stress state before fracture as the materials were assumed linear elastic without assuming any shear fracture criterion [33,34] Table 5.

Table 4
Wave velocity for triplets, as applied for orthotropic planar 2D source localization.

	CM Triplet	Orthotropic Planar 2D location
Horizontal V_x	800–500	$V_x = 500$ m/s, $V_y = 1250$ m/s
Vertical V_y	1250	
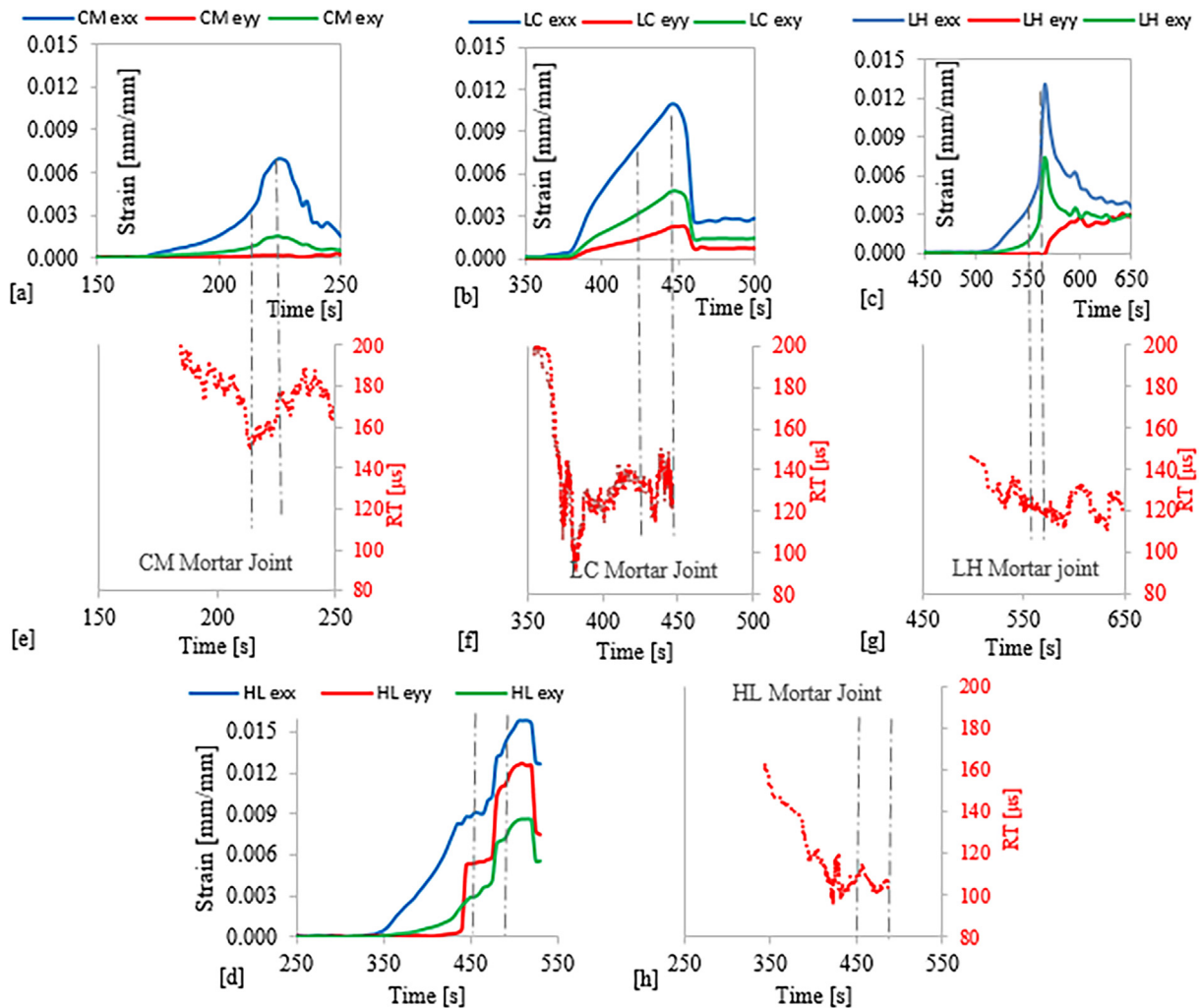
Fig. 8. [a], [b], [c], [d] Strain measurements on (CM, LC, LH, HL) triplets' surface on the crack area, Correlation of each case with the AE characteristics of the cracked area [e], [f], [g], [h].

Table 5
Strain ratios for each triplet composite.

		$\frac{\varepsilon_{xy}}{\varepsilon_{yy}}$ (STDEV)	$\frac{\varepsilon_{xy}}{\varepsilon_{xx}}$ (STDEV)	RT [µs] (STDEV)	AF [kHz] (STDEV)
(CM) Cement Mortar	Numerical	1.29	1.85		
	(70–80)% Load	1.87 (0.66)	0.71 (0.065)	147.57 (10.74)	65.85 (2.45)
	(95–100)% Load	15.98 (2.34)	0.28 (0.045)	180.36 (5.32)	62.56 (1.14)
(LC) Lime Cement (66.7% CL90S)	Numerical	3.88	2.44		
	(70–80)% Load	3.67 (0.36)	0.46 (0.02)	132.66 (6.34)	67.26 (5.48)
	(95–100)% Load	2.64 (0.28)	0.36 (0.058)	121.91 (2.46)	73.31 (3.49)
(LH) Lime Hydrate (100% CL90S)	Numerical	5.11	2.71		
	(70–80)% Load	5.32 (0.42)	0.26 (0.13)	122.46 (5.61)	72.21 (10.19)
	(95–100)% Load	2.24 (0.23)	0.51 (0.12)	114.77 (3.22)	76.61 (12.14)
(HL) Hydraulic Lime	Numerical	8.99	2.86		
	(70–80)% Load	7.52 (1.29)	0.20 (0.13)	114.99 (9.39)	75.03 (7.88)
	(95–100) % Load	0.63 (0.096)	0.56 (0.16)	94.48 (17.11)	79.51 (3.26)

The ratios of the strains depicted in Fig. 8 are calculated and they are tabulated in Table 5. Different normal strain components can be selected in order to bring about interesting correlations with AE parameters. In this section, we focus on $\varepsilon_{xy}/\varepsilon_{yy}$. As this is a shear dominated test, ε_{xy} is the main strain component under investigation. Certain correlations can be conducted with $\varepsilon_{xy}/\varepsilon_{xx}$ as well. The reasons we select to present the ratio $\varepsilon_{xy}/\varepsilon_{yy}$ is that ε_{yy} coincides with the load direction in y axis. Furthermore, the variation of the strain ratio $\varepsilon_{xy}/\varepsilon_{yy}$ is much more characteristic among the different triplet compositions as it presents a higher shift in comparison with the variation of the $\varepsilon_{xy}/\varepsilon_{xx}$ strain ratio. As seen in Table 5, the former ratio varies between 0.7 and 14 for the different binders. However, it was observed that the latter ratio varies only between 0.12 and 0.78.

Moreover, in cases where the level of the different strains is similar, (same order of magnitude between ε_{xx}, ε_{yy}, ε_{xy}) it is reasonable to apply ratios as it is more representative for the different components of strains. In previous studies, stress ratio σ_{xy}/σ_{xx} has yielded very good correlations with AE parameters [35]. However, indeed, when one of the components becomes orders of magnitude higher than the others, then it is reasonable that it dominates the process. For example, for 70–80% of the load, ε_{xx} is much larger ($10E - 3$) than the other two ($10E - 4$ and $10E - 5$) having already overpassed the tensile strain at the cracking (based on our bending experiments). Thus, although the ratio of $\varepsilon_{xy}/\varepsilon_{yy}$ is increasing, this is not dominant as ε_{xx} is extremely high and already exceeding the tensile cracking strain resulting in lower RT. However, for the cases of 95%–100% of the load, the strain components are of the same

order and there, the AE and DIC results seem very consistent with the ratios of strains.

A more illustrative representation of these results is also shown in Fig. 9. Focusing on the AE behavior at the final stage (red bars), it is obvious that the RT of the signals decreases as the cement content and mortar stiffness decreases. Indicatively it is approximately 180 µs for cement binder and reduces to 108 µs for hydraulic lime. This trend is related to a similar trend of the shear strain ratio measured by DIC and shown as "$\varepsilon_{xy}/\varepsilon_{yy}$" in Fig. 9. For cement mortar binder, the shear ratio is quite high (14.4) while for lime it is approximately 0.7. This shows the strong effect of the binder type on the stress distribution and can be explained due to the high deformability that lime imparts on the mortar compositions. It also confirms for masonry the known trend from concrete and other cementitious composites that RT is firmly connected to the stress field that causes the failure [35].

An interesting observation is that the strain field is not constant throughout the loading but changes in a different way depending on the binder type. For CM, the shear ratio strongly increases while for HL it decreases from almost eight to less than one at final failure. For the intermediate cases of LC and LH, there is a moderate decrease of $\varepsilon_{xy}/\varepsilon_{yy}$. It is remarkable that the RT follows these changes closely. For CM, RT increases between first and final stage (from 142 to 180 µs) following the increase of shear proportion from approximately 2–14. For the other types of binders where the shear ratio decreases during the fracture process, the same goes for RT, indicating the sensitivity of AE indices to the developed strain or stress condition. Indicatively, for HL, RT drops from 115 to
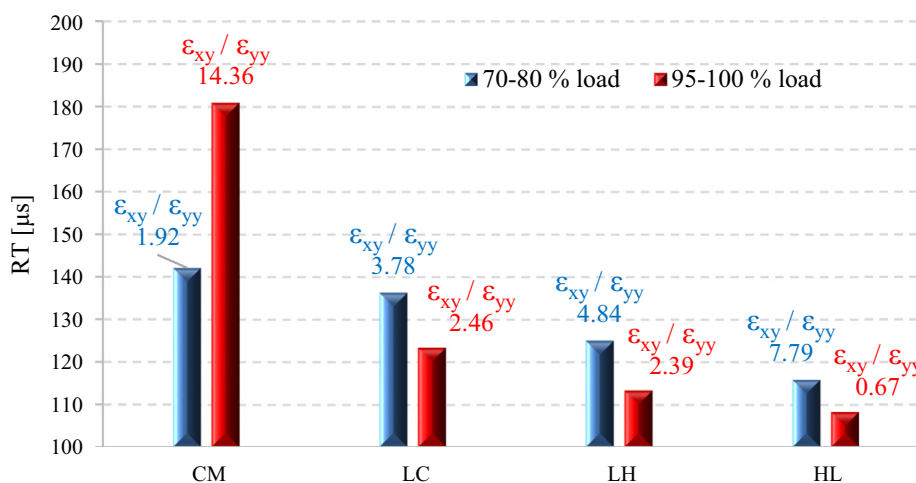
Fig. 9. Rise time and strain ratio ($\varepsilon_{xy}/\varepsilon_{yy}$) evolution in the different triplet compositions for the first and second time intervals.
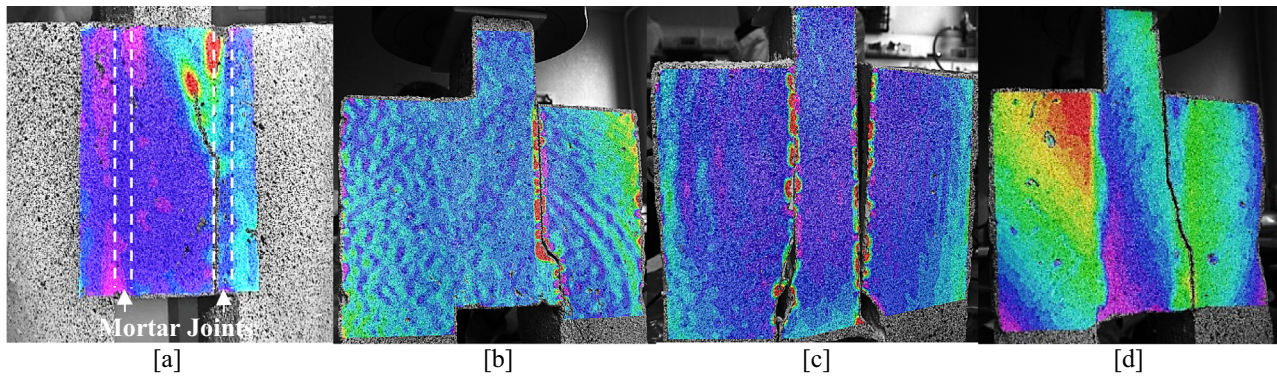
Fig. 10. Masonry triplets – DIC – [a] CM mortar joint – Crack in the interface which propagates also in the brick, [b] LC mortar joint – debonding accompanied with shear mortar failure, [c] LH mortar joint – debonding accompanied with shear mortar failure, [d] HL mortar joint – shear crack propagation through mortar.

108 μs, while the shear strain ratio drops from approximately 8–0.7. In all cases, similar but inverse trends can be seen through average frequency. Reasonably, the range of values is not large due to the resonant behavior of the sensors, but the exact values are also included in Table 5 showing again monotonic correlations to the shear strain ratio. Indicatively for the high shear ratio of CM, the AF is relatively low at 62 kHz while for HL, AF reaches 81 kHz, due to low shear strains.

In order to have a better estimation of the expected strain ratios, similar values were obtained from the FEM analysis in the triplet specimens. As a first approach, in the simulations (Fig. 3) we observe that in the case of CM mortar joint, there is significant strain distribution in the brick as well (this is more obvious in the exy and exx strains). This is because of the higher elastic modulus of the mortar compare to the brick. On the other hand, in the case of HL mortar joint, the strains are undertaken mostly by the mortar joints, which have higher deformability than the brick. Consequently, the different mortar compositions affect significantly the strain distribution and this highlights the importance of a simulation in a strain evaluation. Taking into account that linear elastic properties are assumed in the different finite element models it is worthy to compare the strain ratios with the respective ones arisen from the first time intervals before fracture (70–80% max load) in DIC analysis for a more representative comparison. In Table 5, the average values of all the tests are presented with the respective standard deviations. it is observed that the shear over the vertical normal strain ratio, arisen from numerical simulations, increases constantly from 1.29 to 8.99 with the change of the mortar composition from cement to less stiff lime mortar, in agreement with early DIC measurements where no microcracks alter the triaxial stress state. In the following table AF values are also presented. Their changes accurately follow the opposite trends of the RT values but with smaller differences since the sensors that are used are resonant.

The agreement between numerical and actual DIC strains is good for the early stage of loading, both indicating the increase of shear proportion as the binder softens, even though the exact experimental boundary conditions cannot be used as input. Indeed, in simulations, there is no horizontal restrain and the specimens are free to expand perpendicular to the load direction. In experiments, a horizontal restrain is possible although Teflon sheets are used to minimize this effect. Certainly, after damage has developed, the strain field may well change compared to the original as changes in geometry and cracks evolve on top of the static simulation model.

Similar results, concerning both AE and DIC, have also been produced by the other triplet specimens. Indicatively, the strain ratio $\varepsilon_{xy}/\varepsilon_{yy}$ extracted by the first DIC time interval (70–80 % max load) is increasing from 2.5 to 6.1 for the different binders. The strain ratio for the second time interval close to fracture decreases from 18.6 to 0.7 with a related decrease of RT from 185.4 μs to 99.7 μs and increase of AF from 63.9 kHz to 78.9 kHz as the mortar composition changes from CM towards to HL. Finally, it is observed that the behavior of all triplet specimens is presenting mixed results. Focusing in the Fig. 5[b] where the AE characteristics of the individual constituents are presented, we can see that the behavior of the total AE activity (blue dashed rectangle area) of the triplet specimens is close to the behavior of mortars under bending without being far from the shear characteristics. This can confirm the prior assumption and the later confirmation by DIC that the lack of lateral supports caused horizontal slippage of the edge bricks and as a result bending in the mortar joints contributed to the final failure.

According to the macroscopic observations in Fig. 10, photographs indicate that in CM triplets (Fig. 10[a]), the dominant fracture was interface contact failure combined with brick failure. In the case of LC and LH triplets (Fig. 10[b], [c]), after the shear strain reached the peak value it decreased suddenly as partly interface adhesion and cohesion failure combined with a short crack propagation through the mortar was observed. In the case of HL triplets (Fig. 10[d]), the failure pattern changed as long diagonal cracks through the mortar joints indicated the fracture. In general, it can be stated that for the case of CM, which mechanically is closer to the properties of the brick than the other mortars, the crack is deviated from the interface into the brick, while in the cases of LC, LH and HL the fracture mainly takes place in the mortar width, without propagating into the brick.

5. Conclusions

This study clearly describes how the non-destructive techniques work complementarily on structural materials and specifically on masonry. It Signifies the sensitivity of the AE parameters to the binder, the developed stress field and the fracture mode. In addition, DIC calculates in a non-contact and global manner the strains and the resulted cracks. Initially, UPV measurements provided accurate estimations on the mechanical characteristics and wave propagation of the materials while AE monitoring provided information on the failure mechanisms in masonry constituents and components. AE showed distinct behavior between brick and mortar tests, while individual mortar compositions exhibited different AE characteristics according to their stiffness. More importantly, AE was sensitive to the fracture mode of masonry components, being in strong correlation to the shear over normal strain proportion, as obtained by the DIC strain patterns. The discrepancies in mechanical behavior of the different mortars were measurable through AE and DIC earlier than visible cracking

occurred. The received AE parameters were accurately related to the actual strain of the material at the same time. As a result, a better determination of the universal behavior of the shear effect in masonry was achieved. This complementary verification between the internal fracture process by AE and the surface strain measurements by DIC contributes to a better understanding of masonry behavior. FEM simulations confirmed that the stiffness of the binder crucially affects the developed stress and strain components at early loading stages as confirmed by DIC, without however, being constant until final failure.

Finally, the possibility of influence by the position of sensors in masonry experiments cannot be excluded. It is highly possible that the AE signals undergo strong changes in their propagation path from the source to the receiver. In masonry, there is always reflection on the interfaces and attenuation, which alters the waveforms' shape. As a result, the drop of frequency and increase of the RT is expected [36]. For this reason, simulations are under investigation in order to examine the change of the waveform shape after propagation in masonry components and provide strong basis for a future extrapolation in larger elements [37]. This will be a key consideration in real-scale applications.

Declaration of Competing Interest

None.

Acknowledgments

References

[1] K. Van Balen, I. Papayianni, R. Van Hees, L. Binda, A. Waldum, RILEM TC 167-COM: Characterisation of old mortars with respect to their repair Introduction to requirements for and functions and properties of repair mortars, Mater. Struct. 38 (2005) 781–785.

[2] D.M. McCann, M.C. Forde, Review of NDT methods in the assessment of concrete and masonry structures, NDT and E Int. 34 (2001) 71–84.

[3] A. Saisi, C. Gentile, M. Guidobaldi, Post-earthquake continuous dynamic monitoring of the Gabbia Tower in Mantua Italy, Constr. Build. Mater. 81 (2015) 101–112.

[4] S. Singh, P. Munjal, Bond strength and compressive stress-strain characteristics of brick masonry, J. Build. Eng. 9 (2017) 10–16.

[5] ASTM C 270-07. Standard Specification for Mortar for Unit Masonry. United States: American Society for Testing and Material. 2–13 (2007). doi:10.1520/C0270-14A.

[6] C. Papanicolaou, T. Triantafillou, M. Lekka, Externally bonded grids as strengthening and seismic retrofitting materials of masonry panels, Constr. Build. Mater. 25 (2011) 504–514.

[7] V. Alecci, M. Fagone, T. Rotunno, M. De Stefano, Shear strength of brick masonry walls assembled with different types of mortar, Constr. Build. Mater. 40 (2013) 1038–1045.

[8] N. Mojsilović, G. Simundic, A.W. Page, Static-cyclic shear tests on masonry triplets with a damp-proof course membrane, Proceedings of the 12 th Canadian Masonry Symposium, Vancouver, 2013.

[9] C.U. Grosse, M. Ohtsu, Acoustic Emission Testing – Basic for Research-Applications in Civil Engineering, Springer, Germany Leipzig, 2008.

[10] J.S. Popovics, NDE techniques for concrete and masonry structures, Prog. Struct. Mat. Eng. 5 (2003) 49–59.

[11] M. Wevers, Listening to the sound of materials: Acoustic emission for the analysis of material behaviour, NDT and E Int. 30 (1997) 99–106.

[12] M. Ohtsu, H. Watanabe, Quantitative damage estimation of concrete by acoustic emission, Constr. Build. Mater. 15 (2001) 217–224.

[13] R. Kravchuk, E.N. Landis, Acoustic emission-based classification of energy dissipation mechanisms during fracture of fiber-reinforced ultra-high-performance concrete, Constr. Build. Mater. 176 (2018) 531–538.

[14] G. Lacidogna, A. Manuello, G. Niccolini, Acoustic emission monitoring of Italian historical buildings and the case study of the Athena temple in Syracuse, Archit. Sci. Rev. 58 (4) (2015) 290–299.

[15] S. Iliopoulos, D.G. Aggelis, L. Pyl, J. Vantomme, P. Van Marcke, E. Coppens, L. Areias, Detection and evaluation of cracks in the concrete buffer of the Belgian Nuclear Waste container using combined NDT techniques, Constr. Build. Mater. 78 (2015) 369–378.

[16] G. Lacidogna, G. Piana, A. Carpinteri, Damage monitoring of three-point bending concrete specimens by acoustic emission and resonant frequency analysis, Eng. Fract. Mech. (2018), https://doi.org/10.1016/j.engfracmech.2018.06.034.

[17] H.-L. Nghiem, M. Al Heib, F. Emeriault, Method based on digital image correlation for damage assessment in masonry structures, Eng. Struct. 86 (2015) 1–15.

[18] E. Verstrynge, K. De Wilder, B. Urrego, L. Elvira, E. Voet, K. Van Balen, Advanced Techniques for Monitoring Settlement-Induced Deformations and Crack Growth in Historical Masonry, in: Proceedings of the 10th International Conference on Structural Analysis of Historical Constructions, SAHC2016, 2016, pp. 645–652.

[19] R. Ghorbani, F. Matta, M.A. Sutton, Full-field deformation measurement and crack mapping on confined masonry walls using digital image correlation, Exp. Mech. 55 (2015) 227–243.

[20] E. Verstrynge, K. De Wilder, A. Drougkas, E. Voet, K. Van Balen, M. Wevers, Crack monitoring in historical masonry with distributed strain and acoustic emission sensing techniques, Constr. Build. Mater. 162 (2018) 898–907.

[21] G. Livitsanos, N. Shetty, D. Hündgen, E. Verstrynge, M. Wevers, D. Van Hemelrijck, D.G. Aggelis, Acoustic emission characteristics of fracture modes in masonry materials, Constr. Build. Mater. 162 (2018) 914–922.

[22] E. Verstrynge, L. Schueremans, D. Van Gemert, Time-dependent mechanical behavior of lime-mortar masonry, Mater. Struct. 44 (2011) 29–42.

[23] D. Ferretti, Z.P. Bažant, Stability of ancient masonry towers: Moisture diffusion, carbonation and size effect, Cem. Concr. Res. 36 (2006) 1379–1388.

[24] R. Hendrickx, The Adequate Measurement of the Workability of Masonry Mortar PhD Thesis, Civil Engineering Department, KU Leuven, 2009.

[25] EN 1052-3:2002 Methods of testing cement - Part 1: determination of strength. (2013).

[26] H. Schreier, J.-J. Orteu, M.A. Sutton, Image Correlation for Shape, Motion and Deformation Measurements, Springer US, 2009. doi:10.1007/978-0-387-78747-3.

[27] Abaqus Inc. Abaqus Analysis User Manual. California: Abaqus Inc (2004).

[28] E. Tsangouri, D.G. Aggelis, T.E. Matikas, A.C. Mpalaskas, Acoustic emission activity for characterizing fracture of marble under bending, Appl. Sci. (Switzerland) 6 (2016) 1–12.

[29] T. Shiotani, M. Ohtsu, K. Ikeda, Detection and evaluation of AE waves due to rock deformation, Constr. Build. Mater. 15 (2001) 235–246.

[30] M. Ohtsu, T. Yuichi, Phenomenological Model of Corrosion Process in Reinforced Concrete identified by AE, ACI Mater J 2007 105 (2) (2011) 194–200.

[31] Recommendation of RILEM TC 212-ACD: acoustic emission and related NDE techniques for crack detection and damage evaluation in concrete Test method for classification of active cracks in concrete structures by acoustic emission RILEM Technical Committee. (2010). doi:10.1617/s11527-010-9640-6.

[32] EN 1052-3:2002 Methods of test for mortar masonry - Part 3: Determination of initial shear strength. 3, 14 (2002).

[33] W. Chen, H. Konietzky, C. Liu, H. Fu, J. Zhang, Prediction of Brickwork Failure Using Discrete-Element Method, J. Mater. Civ. Eng. 30 (2018) 6018012.

[34] A. Drougkas, P. Roca, C. Molins, Nonlinear micro-mechanical analysis of masonry periodic unit cells, Int. J. Solids Struct. 80 (2016) 193–211.

[35] J. Blom, M. El Kadi, J. Wastiels, D.G. Aggelis, Bending fracture of textile reinforced cement laminates monitored by acoustic emission: Influence of aspect ratio, Constr. Build. Mater. 70 (2014) 370–378.

[36] D.G. Aggelis, T. Shiotani, A. Papacharalampopoulos, D. Polyzos, The influence of propagation path on elastic waves as measured by acoustic emission parameters, Struct. Health Monit. 11 (2012) 359–366.

[37] G. Livitsanos, N. Shetty, E. Verstrynge, M. Wevers, D. Van Hemelrijck, D.G. Aggelis, Numerical Simulation of Wave Propagation in Masonry, 24th International Acoustic Emission Symposium (IAES), Sapporo, Japan, 2018, pp. 5–9.